International Journal of Numerical Methods for Heat & Fluid Flow

Numerical solution of second law analysis for MHD Casson nanofluid past a wedge with activation energy and binary chemical reaction

Aurang Zaib, Mohammad Mehdi Rashidi, Ali J. Chamkha, Krishnendu Bhattacharyya,

Received 13 February 2017
Revised 4 April 2017
Accepted 8 April 2017

Numerical solution of second law analysis for MHD Casson nanofluid past a wedge with activation energy and binary chemical reaction

Aurang Zaib
Department of Mathematical Sciences, Federal Urdu University of Arts, Science and Technology, Karachi, Pakistan

Mohammad Mehdi Rashidi
Department of Civil Engineering, University of Birmingham, Birmingham, UK

Ali J. Chamkha
Department of Mechanical Engineering, Prince Mohammad Bin Fahd University, Al-Khobar, Saudi Arabia, and

Krishnendu Bhattacharyya
Department of Mathematics, Banaras Hindu University, Varanasi, India

Abstract

Purpose – This paper aims to peruse the influence of second law analysis for electrically conducting fluid of a Casson nanofluid over a wedge. For activation energy, a modified Arrhenius function is used.

Design/methodology/approach – The highly non-linear governing equations are developed using similarity transformations and then computed numerically via Keller–Box method.

Findings – The influences of emerging parameters on velocity, temperature distribution and concentration of nanoparticle are explained and presented via graphs and tables. Also, the behavior of fluid flow is investigated through the coefficient of skin friction, Nusselt and Sherwood numbers. Results reveal that the velocity profile enhances due to increasing Casson parameter and magnetic parameter, whereas the temperature distribution and concentration of nanoparticle decrease with larger vales of Casson parameter. It is inspected that the concentration boundary layer increases due to activation energy and decreases due to reaction rate and temperature differences.

Originality/value – The authors believe that all the numerical results are original and significant which are used in biomedicine, industrial, electronics and transportation. The results have not been considered elsewhere.

Keywords Entropy generation, MHD, Casson nanofluid, Activation energy, Binary chemical reaction, Wedge

Paper type Research paper

Introduction

At present, the impact of non-Newtonian fluids is acknowledged more suitable for technological and scientific applications than Newtonian fluids. In the past, various non-Newtonian fluid models were proposed by researchers due to the fact that all the characteristics

International Journal of Numerical Methods for Heat & Fluid Flow
Vol. 27 No. 12, 2017
pp. 2816-2834

0961-5539
DOI 10.1108/HFF-02-2017-0063

of a non-Newtonian materials cannot be predicted by a single model. The Casson fluid is identified as a non-Newtonian fluid model. This model is the one of best fittest model that expresses the viscoelastic properties in more realistic form than any other models. Few common examples of this model are tomato sauce, jelly, human blood, honey and many more. Also, when blood moves through small vessels at low shear rates, this flow is explained by this model (McDonald, 1974; Shaw *et al.*, 2009). Therefore, it is significant to undertake the study of Casson fluid. Mousavi and Abbasbandy (2011) studied forced convective flow embedded in Darcy–Brinkman–Forchheimer porous medium inside a circular tube with heat flux. The boundary layer flow inside a permeable channel for Darcy–Brinkman equations with suction/injection was scrutinized by Seyf and Mousavi (2011). Shirazpour *et al.* (2011) obtained the analytic solution of fully developed flow in a channel embedded in a Darcy–Brinkman porous medium with Lorentz force. Mustafa *et al.* (2012) scrutinized the steady flow with heat transfer of a Casson fluid near a stagnation-point toward a stretching surface. Shehzad *et al.* (2013) explored the electrically conducting Casson fluid with mass transfer over a permeable stretching surface. The exact solution of flow past a shrinking surface filled with Casson fluid was perceived by Bhattacharyya *et al.* (2014). Mousavi and Yaghoobi (2014) discussed the impact of viscous dissipation in fluid flow embedded in a porous medium in the presence of nonlinear drag term bounded by two isoflux or isothermal walls. Malik *et al.* (2015) inspected the magnetic field on fluid flow of a hyperbolic tangent fluid toward a stretching cylinder. Abolbashari *et al.* (2015) scrutinized the effect of entropy generation on a Casson nanofluid over a heated stretching surface with partial slip. Zaib *et al.* (2016) obtained the dual solutions of Casson fluid with heat transfer toward an exponentially shrinking sheet with viscous dissipation. Mousavi *et al.* (2014) obtained the analytic solution of Maxwell fluid at various wall condition embedded in a porous channel using optimal homotopy analysis method. Recently, Durairaj *et al.* (2017) scrutinized the unsteady flow of a Casson fluid past a vertical cone as well as flat plate embedded in a non-Darcy porous medium with heat generation/absorption and chemical reaction.

Due to the massive applications in modern technology, the nanofluid is a kind of new fluid that has grabbed the attention of distinctive from various authors because of its several applications in biomedicine, industrial, electronics and transportation. Nanofluid is a fluid which is formed by scattering nanometer sized-solid particles and/or fibers having diameter less than 100 nm. Regular heat transfer fluids such as water, bio fluids, engine oil and ethylene glycol have lower thermal conductivities which cannot congregate with the requirement of modern technologies of cooling. Choi and Eastman (1995) dispersed the particles made of metal or metal oxide into regular fluids to improve the thermal conductivity, as the nanofluids thermal conductivity is much larger than the regular or convectional fluids. Buongiorno (2006) observed that the Brownian motion parameter and thermophoresis diffusion effect of nanoparticles give the massive enhancement in the fluids thermal conductivity. Nield and Kuznetsov (2009, 2010) initially examined the boundary layer flow along a vertical surface filled with nanoparticles. Later, Khan and Pop (2010) extended the work of Nield and Kuznetsov by considering a constant surface temperature toward a stretching surface. The impacts of thermophoresis diffusion and Brownian motion over a vertical plate with properties of variable nanofluid were scrutinized by Afify and Bazid (2014). Freidoonimehr *et al.* (2015) scrutinized MHD-free convective flow of a four different water-based nanofluid toward a porous vertical unsteady stretching surface. Liu *et al.* (2016) developed an approach containing optomechanical actuator nanoparticle to control tension receptor optically in living cells. The reliability of dual embedded atom method based on copper, aluminum and nickel interatomic potentials for predicting the elastic properties was investigated by Mousavi *et al.* (2014). Afify and Elgazery (2016)

explored the influence of electrically conducting Maxwell fluid past a stretching sheet with chemical reaction and nanoparticles. Recently, Khan *et al.* (2017) discussed the magnetic field with nonlinear radiation effect on boundary layer flow of a nanofluid past a permeable wedge.

Various systems dealing heat transfer with the mechanism of irreversibility which illustrates the entropy generation are corresponds to mass transfer, viscous dissipation, heat transfer and magnetic field. Different researchers/scientists applied the second law of thermodynamics (Bejan, 1980, 1996; Galanis and Rashidi, 2012). To optimize such kind of irreversibility, for instance, Mahmud and Fraser (2004) considered the MHD-free convection flow with entropy generation through a porous cavity. They determined that increment in a magnetic field leads to increase the entropy generation. Further investigation of entropy generation under the influence of MHD and slip flow on a rotating disk in a porous medium having variables properties, was given by Rashidi *et al.* (2014). Shateyi *et al.* (2015) scrutinized the second law analysis on electrically conducting Maxwell fluid toward a stretching surface embedded in porous medium. Recently, numerical study was conducted by Qing *et al.* (2016) on entropy generation. They discussed the Casson fluid flow toward a stretching/shrinking porous surface.

The process of mass transfer with Arrhenius activation energy and binary chemical reaction has been given a lot of consideration because of its several applications in chemical engineering, cooling of nuclear reacting, geothermal reservoirs and recovery of thermal oil. Generally, the relations between chemical reactions and mass transport are very complex and can be scrutinized in the utilization of species of reactant and production at several rates within the mass transfer and fluid. Bestman (1990) was first who considered the combined effects of binary chemical reaction and Arrhenius activation energy on free convective flow with mass transfer in a vertical pipe immersed in a porous medium. He obtained the analytic solution using perturbation method. Maleque (2013) studied MHD-free convection flow and heat with mass transfer past a porous vertical plate with binary chemical reaction and Arrhenius activation energy with viscous dissipation and heat generation\absorption. The boundary layer flow and heat transfer using two-equation energy model inside a channel embedded in porous medium was investigated by Mousavi *et al.* (2013). Awad *et al.* (2014) scrutinized an unsteady flow in a rotating fluid past a stretching sheet with binary chemical reaction and Arrhenius activation energy.

The current research aims to scrutinize the entropy generation on MHD Casson fluid flow containing nanoparticles past a wedge with activation energy and binary chemical reaction. Similarity equations are developed and obtained numerical solution via Keller–Box method. The influences of emerging parameters on fluid velocity, temperature distribution and concentration of nanoparticle are examined through graphs to discuss the important features of the fluid flow. The impacts of skin friction, Nusselt and Sherwood numbers are displayed in the tables. This kind of problem is yet not considered.

Problem formulation

Consider a steady two-dimensional incompressible fluid toward the stagnation point of Casson nanofluid over a wedge as shown in Figure 1. Activation energy with binary chemical reaction are invoked. It is considered that external velocity $\widehat{u}_e(\widehat{x}) = c\widehat{x}^{\,n}$ varies non-linearly from the stagnation-point. Further, wall temperature $\widehat{T}_w$ and wall concentration $\widehat{C}_w$ as well ambient temperature $\widehat{T}_\infty$ and ambient concentration $\widehat{C}_\infty$ are considered as constant. For an isotropic flow, the rheological sate equation of Casson fluid is expressed as (Shehzad *et al.*, 2013; Hayat *et al.*, 2012):

$$\hat{\tau}_{ij} = \begin{cases} \left(\hat{\mu}_B + \dfrac{\hat{p}_y}{\sqrt{2\hat{\pi}}}\right) 2\hat{e}_{ij}, & \hat{\pi} > \hat{\pi}_c, \\ \left(\hat{\mu}_B + \dfrac{\hat{p}_y}{\sqrt{2\hat{\pi}_c}}\right) 2\hat{e}_{ij}, & \hat{\pi} < \hat{\pi}_c, \end{cases} \tag{1}$$

where $\hat{\pi} = \hat{e}_{ij}\hat{e}_{ij}$ with $\hat{e}_{ij}$ are the (i, j)th components of rate of deformation, $\hat{\pi}$ is product of the component of rate of deformation with itself, $\hat{\pi}_c$ is the critical value of the product of the component of the strain tensor rate with itself, $\hat{\mu}_B$ is the dynamic viscosity of Casson fluid and $\hat{p}_y$ is the yield stress of fluid. The governing equations using the approximation of boundary layer with the above assumptions are described as:

$$\frac{\partial \hat{u}}{\partial \hat{x}} + \frac{\partial \hat{v}}{\partial \hat{y}} = 0 \tag{2}$$

$$\hat{u}\frac{\partial \hat{u}}{\partial \hat{x}} + \hat{v}\frac{\partial \hat{u}}{\partial \hat{y}} - \hat{u}_e\frac{d\hat{u}_e}{d\hat{x}} = \hat{\nu}\left(1 + \frac{1}{\gamma}\right)\frac{\partial^2 \hat{u}}{\partial \hat{y}^2} - \frac{\tilde{\sigma}\tilde{B}_0^2}{\tilde{\rho}}(\hat{u} - \hat{u}_e) \tag{3}$$

$$\hat{u}\frac{\partial \hat{T}}{\partial \hat{x}} + \hat{v}\frac{\partial \hat{T}}{\partial \hat{y}} = \hat{\alpha}\frac{\partial^2 \hat{T}}{\partial \hat{y}^2} + \Lambda\left[\hat{D}_B\frac{\partial \hat{C}}{\partial \hat{y}}\frac{\partial \hat{T}}{\partial \hat{y}} + \left(\frac{\hat{D}_T}{\hat{T}_\infty}\right)\left(\frac{\partial \hat{T}}{\partial \hat{y}}\right)^2\right] \tag{4}$$

$$\hat{u}\frac{\partial \hat{C}}{\partial \hat{x}} + \hat{v}\frac{\partial \hat{C}}{\partial \hat{y}} = \hat{D}_B\frac{\partial^2 \hat{C}}{\partial \hat{y}^2} + \left(\frac{\hat{D}_T}{\hat{T}_\infty}\right)\left(\frac{\partial^2 \hat{T}}{\partial \hat{y}^2}\right) - \hat{k}_r^2\left(\frac{\hat{T}}{\hat{T}_\infty}\right)^{n_1} e^{-\frac{\hat{E}_a}{\kappa \hat{T}}}(\hat{C} - \hat{C}_\infty) \tag{5}$$

The physical boundary conditions are:

$$\begin{aligned} &\hat{u} = 0, \hat{v} = 0, \hat{T} = \hat{T}_w, \hat{C} = \hat{C}_w \text{ at } \hat{y} = 0, \\ &\hat{u} \to \hat{u}_e(\hat{x}), \hat{T} \to \hat{T}_\infty, \hat{C} \to \hat{C}_\infty \text{ as } \hat{y} \to \infty \end{aligned} \tag{6}$$

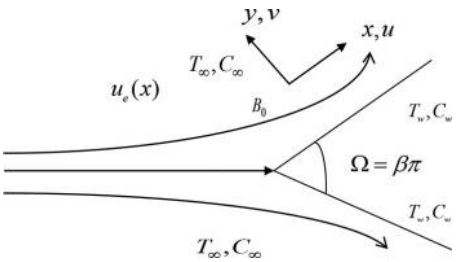

Figure 1.
Flow diagram past a wedge

where $\widehat{u}$ and $\widehat{v}$ are components of velocity in $\widehat{x}-$ and $\widehat{y}-$ directions, respectively; $\gamma = \widehat{\mu}_B\sqrt{2\widehat{\pi}_c}/\widehat{p}_y$ is the Casson parameter; $\widehat{\nu}$ is the kinematic viscosity; $\tilde{\rho}$ is the density; $\widehat{\alpha}$ is the thermal diffusivity; $\tilde{\sigma}$ is the electrical conductivity; $\tilde{B}_0$ is the induction of magnetic field; $\widehat{T}$ is the temperature; $\widehat{T}_\infty$ is the ambient temperature; $\widehat{C}$ is the concentration of nanoparticle; $\widehat{D}_B$ and $\widehat{D}_T$ are the coefficients of Brownian and thermophoresis diffusion, respectively; Λ is the ratio of the nanoparticle effective heat capacity to base fluid specific heat capacitance; $\widehat{k}_r^2(\widehat{T}/\widehat{T}_\infty)^{n_1}e^{-\frac{\widehat{E}_a}{\kappa\widehat{T}}}$ and κ are the function of modified Arrhenius and the Boltzmann constant, respectively, where $\widehat{k}_r^2$ is the rate constant of chemical reaction and n_1 is the fitted rate constant lies between $-1 < n_1 < 1$.

Now, we introduce the similarity transformation:

$$\eta = \widehat{y}\sqrt{\frac{c(n+1)}{2\widehat{\nu}}}\widehat{x}^{\frac{n-1}{2}},\quad \psi = \sqrt{\frac{2c\widehat{\nu}}{(n+1)}}\widehat{x}^{\frac{n+1}{2}}f(\eta),\quad \theta(\eta) = \frac{\widehat{T}-\widehat{T}_\infty}{\widehat{T}_w-\widehat{T}_\infty},$$

$$\phi(\eta) = \frac{\widehat{C}-\widehat{C}_\infty}{\widehat{C}_w-\widehat{C}_\infty} \tag{7}$$

Here, η is the similarity variable, ψ is the stream function.

In view of relation (7), equations (3)-(6) are transmuted to:

$$\left(1+\frac{1}{\gamma}\right)f''' + ff'' + \beta\left(1-f'^2\right) + M^2\frac{2}{(n+1)}(1-f') = 0 \tag{8}$$

$$\theta'' + \Pr f\theta' + \Pr Nb\theta'\phi' + \Pr Nt(\theta')^2 = 0 \tag{9}$$

$$\phi'' + Scf\phi' + \frac{Nt}{Nb}\theta'' - \beta_1 Sc(1+\delta\theta)^{n_1}\exp\left(-\frac{E}{1+\delta\theta}\right)\phi = 0 \tag{10}$$

subject to the boundary conditions:

$$\begin{aligned} &f(0) = 0,\ f'(0) = 0,\ \theta(0) = 1,\ \phi(0) = 1,\\ &f'(\infty)\to 1,\ \theta(\infty)\to 0,\ \phi(\infty)\to 0 \end{aligned} \tag{11}$$

where prime indicate the differentiation to η, $M^2 = \tilde{\sigma}\tilde{B}_0^2\widehat{x}^{1-n}/\tilde{\rho}c$ is the magnetic parameter, $\beta = 2n/(1+n)$ is the wedge angle parameter, $Nb = \Lambda\widehat{D}_B(\widehat{C}_w-\widehat{C}_\infty)/\tilde{\nu}$ is the Brownian motion parameter, $Nt = \Lambda\widehat{D}_T(\widehat{T}_w-\widehat{T}_\infty)/\widehat{T}_\infty\widehat{\nu}$ is the thermophoresis parameter, $E = \widehat{E}_a/\kappa\widehat{T}_\infty$ is the dimensionless activation energy, $\beta_1 = \widehat{k}_r^2/c\widehat{x}^{n-1}$ is the non-dimensional reaction rate, $\delta = (\widehat{T}_w-\widehat{T}_\infty)/\widehat{T}_\infty$ is the temperature difference parameter and $Sc = \widehat{\nu}/\widehat{D}_B$ is the Schmidt number. It is worth mentioning that the value of

$n = 0$ ($\beta = 0$) represents the flow over a horizontal plate, whereas $n = 1$ ($\beta = 1$) implies flow over a vertical plate.

The significant physical quantities are the skin friction coefficient, Nusselt and Sherwood Numbers are written as:

$$C_{fx} = \frac{\tilde{\tau}_w}{\tilde{\rho}\hat{u}_e^{\,2}}, \quad Nu_x = -\frac{\hat{x}\,\tilde{q}_w}{k(\hat{T}_w - \hat{T}_\infty)}, \quad Sh_x = \frac{\hat{x}\,\tilde{m}_w}{\hat{D}_B(\hat{C}_w - \hat{C}_\infty)} \tag{12}$$

where shear stress $\tilde{\tau}_w$, heat flux $\tilde{q}_w$ and mass flux $\tilde{m}_w$ given as:

$$\tilde{\tau}_w = \left(\hat{\mu}_B + \frac{\hat{p}_y}{\sqrt{2\hat{\pi}}}\right)\left(\frac{\partial \hat{u}}{\partial \hat{y}}\right)_{\hat{y}=0}, \quad \tilde{q}_w = -k\left(\frac{\partial \hat{T}}{\partial \hat{y}}\right)_{\hat{y}=0}, \quad \tilde{m}_w = -\hat{D}_B\left(\frac{\partial \hat{C}}{\partial \hat{y}}\right)_{\hat{y}=0} \tag{13}$$

Using equation (7), we get:

$$\begin{aligned} &C_f\,\mathrm{Re}_x^{1/2} = \sqrt{\frac{n+1}{2}}\left(1+\frac{1}{\gamma}\right)f''(0), \quad Sh_x\,\mathrm{Re}_x^{-1/2} = -\sqrt{\frac{n+1}{2}}\phi'(0), \\ &Nu_x\,\mathrm{Re}_x^{-1/2} = -\sqrt{\frac{n+1}{2}}\theta'(0) \end{aligned} \tag{14}$$

where $\mathrm{Re}_x = \hat{x}\,\hat{u}_e/\hat{\nu}$ is the Reynolds number.

Entropy generation analysis

Entropy equation of the Casson nanofluid is described as:

$$\begin{aligned} S'''_{gen} = {} & \frac{k}{\hat{T}_\infty^{\,2}}\left(\frac{\partial \hat{T}}{\partial \hat{y}}\right)^2 + \frac{\mu}{\hat{T}_\infty}\left(1+\frac{1}{\gamma}\right)\left(\frac{\partial \hat{u}}{\partial \hat{y}}\right)^2 + \frac{\tilde{\sigma}\tilde{B}_0^2}{\hat{T}_\infty}\hat{u}^{\,2} + \frac{RD}{\hat{C}_\infty}\left(\frac{\partial \hat{C}}{\partial \hat{y}}\right)^2 \\ & + \frac{RD}{\hat{T}_\infty}\left(\frac{\partial \hat{T}}{\partial \hat{y}}\right)\left(\frac{\partial \hat{C}}{\partial \hat{y}}\right) \end{aligned} \tag{15}$$

Volumetric entropy generation have two factors, (i) Heat Transfer Irreversibility (HTI) and (ii) Fluid friction Irreversibility (FFI) (iii) Diffusive Irreversibility. It is characterized as:

$$S'''_0 = \frac{k\left(\Delta \hat{T}\right)^2}{L^2\hat{T}_\infty^{\,2}} \tag{16}$$

in dimensionless form:

$$N_G = \frac{S'''_{gen}}{S'''_0} = \frac{(n+1)}{2}\frac{\mathrm{Re}_L Br}{\Omega}\left(1+\frac{1}{\gamma}\right)f''^2 + \frac{(n+1)}{2}\mathrm{Re}_L\theta'^2 + \frac{\mathrm{Re}_L Br}{\Omega}M^2 f'^2 + \frac{(n+1)}{2}\mathrm{Re}_L\lambda\left(\frac{\zeta}{\Omega}\right)^2\phi'^2 + \frac{(n+1)}{2}\mathrm{Re}_L\lambda\left(\frac{\zeta}{\Omega}\right)\theta'\phi' \quad (17)$$

where $\Omega = \Delta\widehat{T}/\widehat{T}_\infty$ is the dimensionless temperature difference, $Br = \mu\widehat{u}_e^2/k\Delta\widehat{T}$ the Brinkman number, $\mathrm{Re}_L = cL^2/v$ is the Reynolds number based on the characteristic length, $\zeta = \Delta\widehat{C}/\widehat{C}_\infty$ is the dimensionless concentration difference and $\lambda = RD\widehat{C}_\infty/k$ is the diffusive constant parameter.

Solution procedure

In the current study, a useful implicit finite difference scheme, namely, Keller–Box method has been used to scrutinize the flow problem described by the transformed equations (8)-(11). This method is widely used to solve the parabolic equations as described in the book of Cebeci and Bradshaw (1988). The summary of this method is given below in four steps:

(1) using new dependent variables to transform the equations (8)-(11) to a first order system;

(2) using central differences to write the difference equation;

(3) using Newton's method to linearize the transformed algebraic equations and then write these equations in matrix vector form; and

(4) with the use of block tri-diagonal elimination method to solve the obtained linear system.

The step size is taken as $\Delta\eta = 0.01$ and obtained the corrected results up to desire accuracy of the level 10^{-5}, that fulfills the criterion of convergence. The satisfied outer boundary condition is obtained by taking the thickness of boundary layer $\eta_\infty = 10$. To check the correctness of the present method, results are affirmed with previous results in the literature illustrated in Tables I and II. It is observed that the present results are matched closely, which assured the validity of the current methodology. Table III displayed the impact of Falkner–Skan power law parameter n on the skin friction, Nusselt and Sherwood numbers versus γ. It can be seen that enhancing the values of n is to boost the skin friction as well as Nusselt number and Sherwood number. Whereas the skin friction significantly reduces by enhancing Casson parameter, the opposite trend is observed on the Nusselt and Sherwood numbers. Moreover, the skin friction, the Nusselt and the Sherwood numbers are positive indicating that fluid exert a drag force on the wedge, whereas heat and mass is moved from the hot surface to the cold fluid.

Table I. Comparison of $f''(0)$ for different n when $M = 0$, $\gamma \to \infty$, $\beta = 2n/(1+n)$

n	Yih (1998)	Yacob *et al.* (2011)	Present
0	0.469600	0.4696	0.4696
1/11	0.654979	0.6550	0.6550
0.2	0.802125	0.8021	0.8021
1/3	0.927653	0.9277	0.9277
0.5		1.0389	1.0389
1	1.232588	1.2326	1.2326

Results and discussion

This section depicts the impacts of several parameters involving in fluid flow problem are discussed through graphs. Figures 2-4 give the impact of Casson parameter γ on the velocity profile, temperature distribution and concentration of nanoparticle for $\beta = 0$ and $\beta = 1$. Figure 2 shows an increasing behavior in velocity profile with increasing values of γ. Thus, Casson parameter reduces the thickness of velocity boundary layer. Physically, the yield stress reduces due to increasing values of γ that decline of velocity boundary layer. On the other hand the temperature distribution and concentration of nanoparticle decrease due to increasing values of γ as shown in Figures 3 and 4, respectively. The thinning of the thermal as well as the concentration boundary layers thicknesses happen due to elasticity

Pr	β	White (1991)	Mutlag *et al.* (2013)	Present
0.1	0	0.1980	0.198033	0.1980
	0.3	0.2090	0.209076	0.2090
	2.0	0.2260	0.226002	0.2260
0.72	0	0.4178	0.418091	0.4181
	0.3	0.4592	0.459551	0.4596
	2.0	0.5292	0.529607	0.5296
1.0	0	0.4690	0.469600	0.4696
	0.3	0.5195	0.519518	0.5195
	2.0	0.6052	0.605197	0.6052
2.0	0	0.5972	0.597233	0.5972
	0.3	0.6690	0.669044	0.6690
	2.0	0.7959	0.795991	0.7960
3.0	0	0.6859	0.685961	0.6860
	0.3	0.7739	0.773436	0.7734
	2.0	0.9303	0.930351	0.9304
10	0	1.0297	1.029747	1.0298
	0.3	1.1791	1.179129	1.1791
	2.0	1.4557	1.455749	1.4558

Table II. Comparison of $-\theta'(0)$ for different β and Pr when $Nb = Nt = 0$, $\gamma \to \infty$

γ	n	$C_f \mathrm{Re}_x^{1/2}$	$Nu_x \mathrm{Re}_x^{-1/2}$	$Sh_x \mathrm{Re}_x^{-1/2}$
0.1	0	1.2851	0.2169	0.2523
	0.3	2.4554	0.2836	0.3031
	0.5	3.0170	0.3161	0.3309
	1	4.1081	0.3819	0.3901
0.2	0	0.8644	0.2321	0.2595
	0.3	1.7955	0.3094	0.3159
	0.5	2.2178	0.3448	0.3453
	1	3.0292	0.4161	0.4072
0.4	0	0.6474	0.2516	0.2693
	0.3	1.3703	0.3345	0.3287
	0.5	1.6934	0.3721	0.3590
	1	2.3135	0.4478	0.4231
0.6	0	0.5646	0.2627	0.2750
	0.3	1.1961	0.3475	0.3353
	0.5	1.4782	0.3861	0.3661
	1	2.0194	0.4640	0.4310

Table III. Values of the skin friction, the Nusselt number and the Sherwood number versus γ for different values of n when $M = 0.1$, $Nb = Nt = 0.1$, $\mathrm{Pr} = Sc = 1$, $E = 5$, $\beta_1 = 3$, $\delta = n_1 = 0.5$ are fixed and $\beta = 2n/(1+n)$

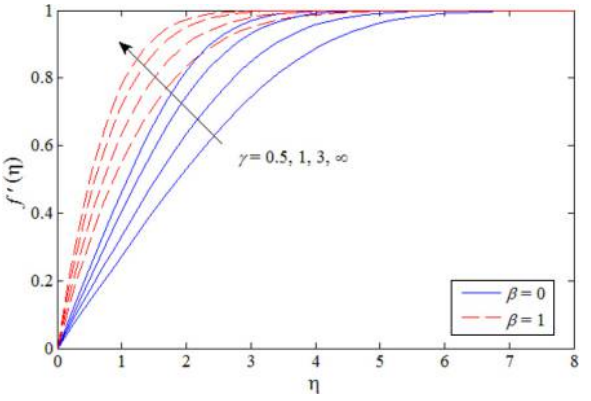

Figure 2.
Velocity profile for different values of γ when $M = 0.1$

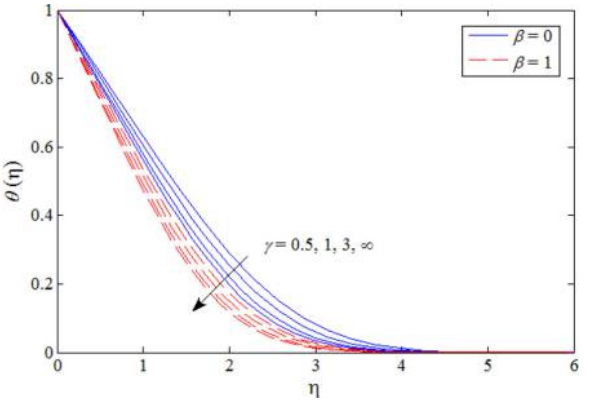

Figure 3.
Temperature profile for different values of γ when $Nb = Nt = 0.1$, $\Pr = 1$

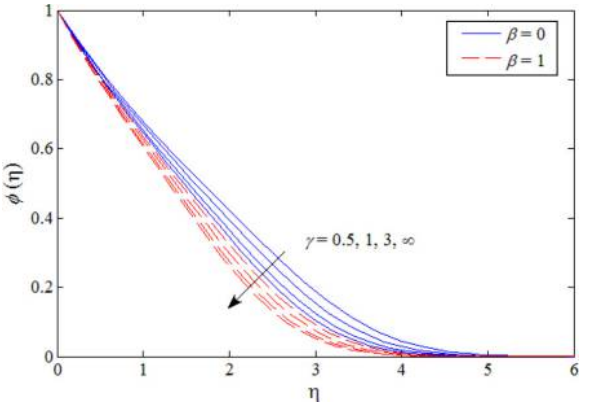

Figure 4.
Concentration of nanoparticle for different values of γ when $Nb = Nt = 0.1$, $\Pr = Sc = 1$, $\beta_1 = 3$, $E = 4$, $n_1 = \delta = 0.5$

stress parameter. It is also seen from these visualizations that as we enhance the Casson parameter, i.e. $\gamma \to \infty$, the behavior of non-Newtonian fluid vanishes and behaves as Newtonian fluid. Further, the thicknesses of velocity, thermal and concentration boundary layers are smaller for Casson fluid compared to Newtonian fluid. Furthermore, the thicknesses of boundary layers are larger for flow over a horizontal plate compared to flow over a vertical plate.

Figure 5 scrutinizes the influence of magnetic parameter M on velocity distribution for Newtonian and non-Newtonian fluids. It is clear that the velocity of fluid and the velocity boundary layer shrink with enhancing M for both fluids. This is due to the fact that the magnetic field is normal to the fluids direction, as the magnetic force in an opposite direction of flow which leads to increase the absorption of stationary fluid on the wedge and declines the speed of flow. Therefore, the flow becomes heavier that needs further time to move. Moreover, velocity boundary layer is thicker in case of non-Newtonian fluid compared to Newtonian fluid.

The influence of wedge angle parameter β on the velocity profile, temperature distribution and concentration of nanoparticle are portrayed in Figures 6-8. Figure 6 illustrates that enlarging β leads to an acceleration in the velocity distribution and consequently thinning the velocity boundary layer. Physically, β implies the pressure

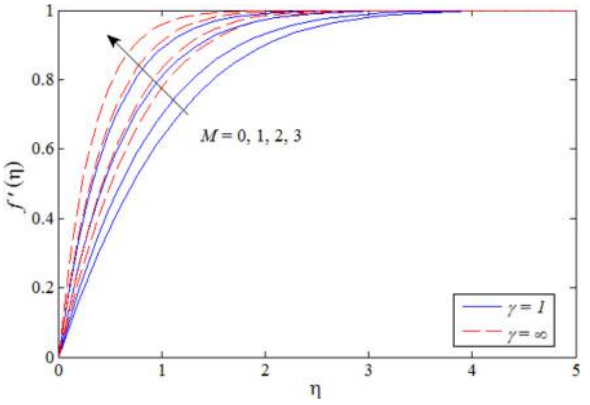

Figure 5.
Velocity profile for different values of M when $\beta = 1$

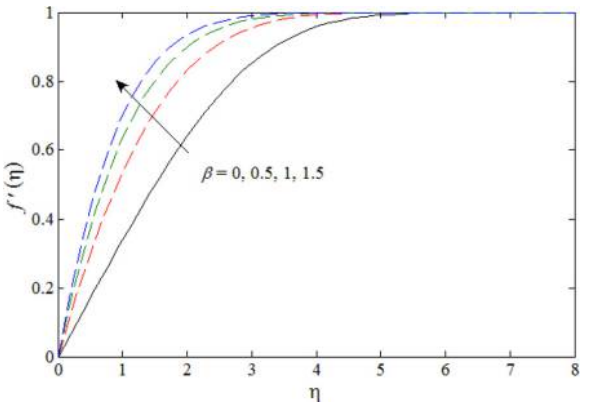

Figure 6.
Velocity profile for different values of β when $M = 0.1$, $\gamma = 1$

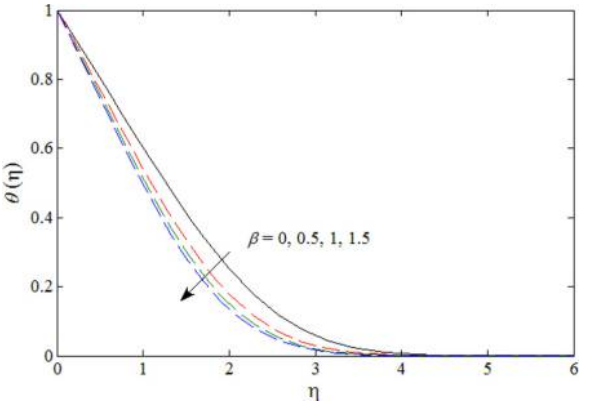

Figure 7.
Temperature profile for different values of β when $\gamma = 1$, $Nb = Nt = 0.1$, $\mathrm{Pr} = 1$

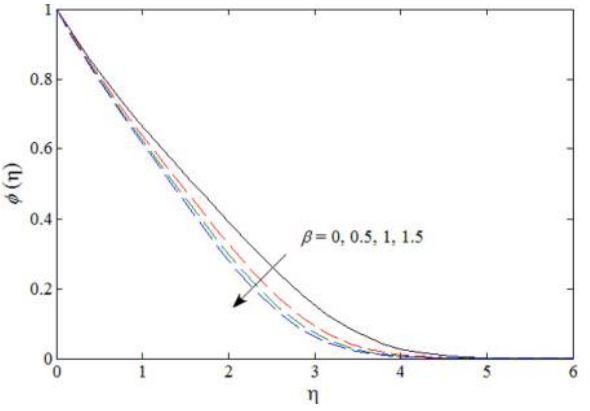

Figure 8.
Concentration of nanoparticle for different values of β when $\gamma = 1$, $Nb = Nt = 0.1$, $\mathrm{Pr} = Sc = 1$, $\beta_1 = 3$, $E = 4$, $n_1 = \delta = 0.5$

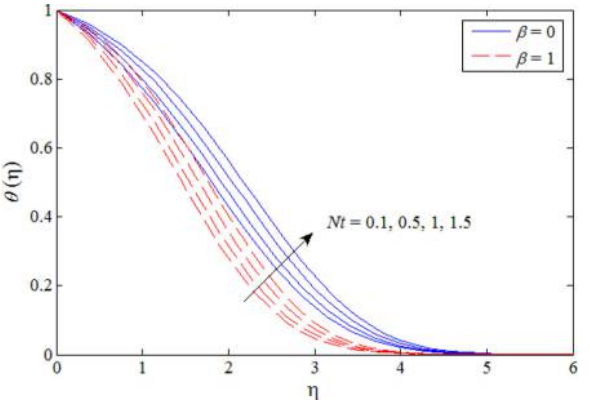

Figure 9.
Temperature profile for different values of Nt when $\gamma = 0.5$, $Nb = 1.5$, $\mathrm{Pr} = 1$

gradient; therefore, positive values indicating a favorable pressure gradient which enhances the flow within the boundary. Due to this, the velocity profile crushes nearer and closer to the wedge and does not happen the reverse flow. On the other hand, the temperature distribution and concentration of nanoparticle decreases by extending β as depicted in Figures 7 and 8, respectively.

The impact of thermophoresis parameter Nt on the temperature distribution and concentration nanoparticle is presented in Figures 9 and 10, respectively. Figures 9 and 10 elucidate that the temperature distribution and concentration nanoparticle enhance with increasing Nt. This is because diffusion penetrates deeper into the fluid due to increasing values of Nt which causes the thickening of the thermal boundary layer as well as the concentration boundary layer. It is interesting to note that the effect of thermophoresis parameter is more pronounced on the concentration of nanoparticle compared to temperature distribution. Figures 11 and 12 are prepared to see the Brownian motion effect Nb on the temperature distribution and concentration of nanoparticle, respectively. Figure 11 reveals that the temperature distribution and thermal boundary layer thickness increase with larger values of Nb. Physical reason is

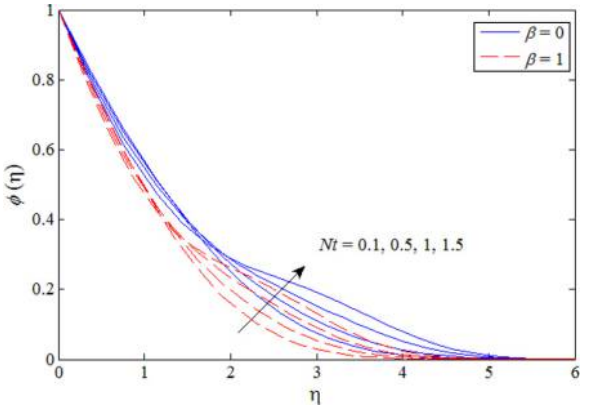

Figure 10.
Concentration of nanoparticle for different values of Nt when $\gamma = 0.5$, $Nb = 1.5$, $\Pr = Sc = 1$, $\beta_1 = E = 6$, $n_1 = \delta = 0.5$

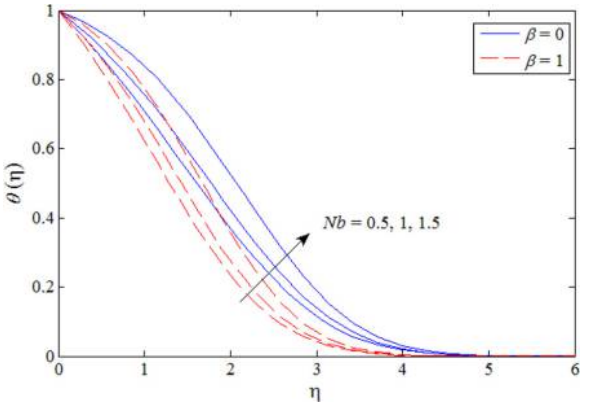

Figure 11.
Temperature profile for different values of Nb when $\gamma = 0.5$, $Nt = 0.5$, $\Pr = 1$

that the kinetic energy of the nanoparticles increases due to the strength of this chaotic motion and, as a result, the fluid's temperature increases. Whereas the opposite trend is seen on the concentration of nanoparticle as depicted in Figure 12. It can be seen that the concentration of nanoparticle decreases due to increasing values of *Nb*. It can be concluded that the Brownian motion parameter makes the fluid warm within the boundary and at that time aggravates deposition particles away from the regime of fluid to the surface, causing in a decrease in concentration of nanoparticle as well as the thickness of boundary layer. The larger values of Brownian motion imply the strong behavior for the smaller particle, whereas the for stronger particle, the smaller values of *Nb* are applied.

Figure 13 shows that due to increasing values of dimensionless reaction rate β_1, the concentration of nanoparticle decreases and leads to thinning the concentration boundary layer thickness. Physically, increasing the value of β_1 guides an increment in the term $\beta_1(1+\delta\theta)^{n_1}\exp(-E/1+\delta\theta)$. This ultimately helps the destructive chemical reaction that increases the concentration. Figure 14 elucidates the increasing behavior in

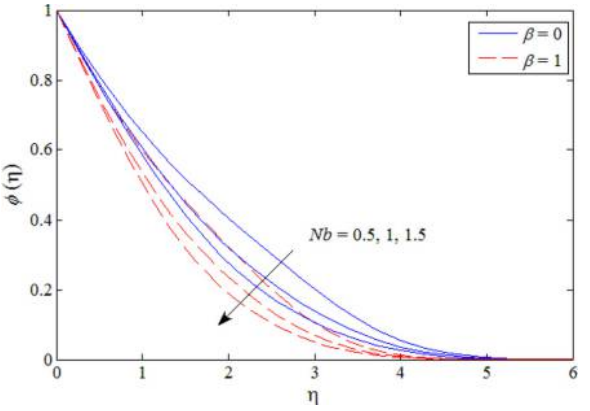

Figure 12.
Concentration of nanoparticle for different values of *Nb* when $\gamma = 0.5$, $Nt = 0.5$, $\Pr = Sc = 1$, $\beta_1 = E = 8$, $n_1 = \delta = 0.5$

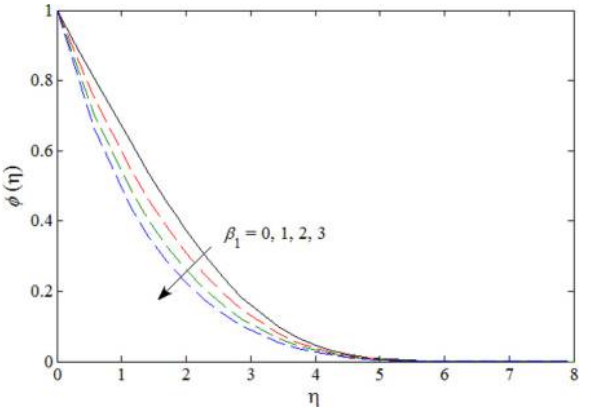

Figure 13.
Concentration of nanoparticle for different values of β_1 when $\gamma = 0.1$, $Nt = Nb = 0.1$, $\beta = 1$, $Pr = \mathrm{Sc} = 1$, $E = 8$, $n_1 = \delta = 0.5$

concentration nanoparticle due to increasing values of non-dimensional activation energy E and leads to increase the concentration boundary layer thickness. Physically, higher activation energy and lower temperature leads to lesser reaction rate which slowdowns the chemical reaction. Figure 15 preserves the influence of temperature difference δ on the concentration of nanoparticle. This result showed that the concentration of nanoparticle and boundary layer decreases due to increasing values of δ.

Figures 16-19 elaborate the variation of entropy generation for selected values of Casson parameter γ, magnetic parameter M, Reynolds number Re_L and Brinkman number Br. Figure 16 envisages that the entropy profile shows a decreasing behavior with increasing γ. As expected, the entropy generation profile is larger for non-Newtonian fluid than Newtonian fluid. Figure 17 reveals that the entropy generation enhances due to larger values of magnetic parameter. A raise in the intensity of magnetic field which enhances the entropy profile. In addition, it perceives that magnetic field is a source entropy generation to the friction of fluid and heat transfer. It can be finalized that the entropy generation can be controlled by taking a small magnetic parameter which is

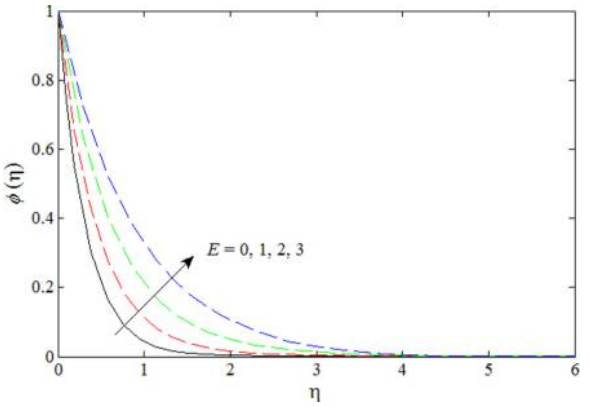

Figure 14.
Concentration of nanoparticle for different values of E when $\gamma = 0.1, Nt = Nb = 0.1, \beta = 1,$ $\mathrm{Pr} = Sc = 1, \beta_1 = 8,$ $n_1 = \delta = 0.5$

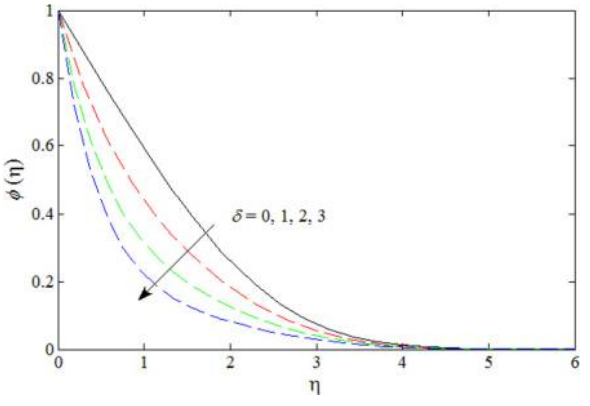

Figure 15.
Concentration of nanoparticle for different values of δ when $\gamma = 0.1, Nt = Nb = 0.1, \beta = 1, \mathrm{Pr} = Sc = 1, E = \beta_1 = 8,$ $n_1 = 0.5$

an important issue in propulsion of MHD nuclear. We perceived from Figures 18 and 19 that entropy profile accelerates by increasing either Brinkman number or Reynolds number. The entropy generation generated from mechanisms of all irreversibilities, and as a result, the entropy generation increases with increasing Re_L. Larger values in entropy generation created by the irreversibility of fluid friction occurs due to increasing Br.

Concluding remarks

The influence of electrically conducting fluid on a non-Newtonian Casson fluid containing nanoparticles over a wedge was explored numerically. The governing equations are developed using similarity transformations into ordinary differential equations before being solved numerically via Keller–Box method. Some significant features of the problem regarding the various pertinent parameters were gathered. The velocity profile enhances

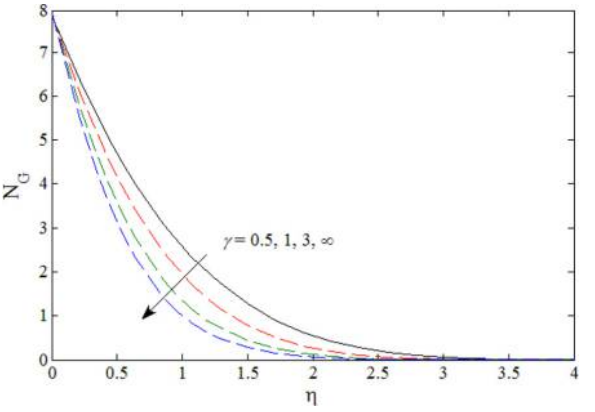

Figure 16.
Entropy generation for different values of γ when $\beta = 1$, $Nt = Nb = 0.1$, $M = 0.1$, $\mathrm{Pr} = Sc = 1$, $\beta_1 = 3$, $E = 5$, $n_1 = 0.5$, $\delta = 0.5$, $\mathrm{Re}_L = Br = 1$, $\zeta = 0.2$, $\lambda = \Omega = 0.01$

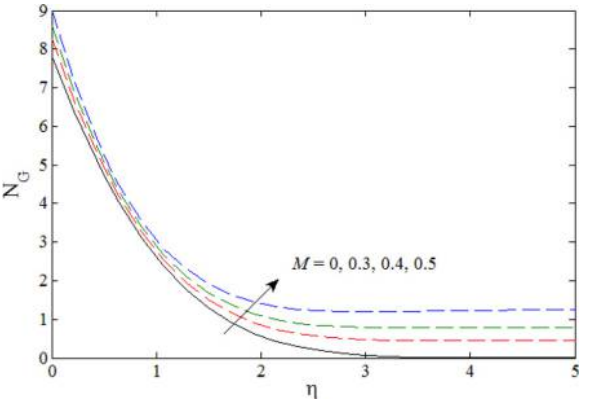

Figure 17.
Entropy generation for different values of M when $\beta = 1$, $Nt = 0.1$, $Nb = 0.1$, $\gamma = 0.5$, $\mathrm{Pr} = Sc = 1$, $\beta_1 = 3$, $E = 5$, $n_1 = 0.5$, $\delta = 0.5$, $\mathrm{Re}_L = Br = 1$, $\zeta = 0.3$, $\lambda = \Omega = 0.01$

due to larger values of γ for flow over a vertical plate as well as flow over a horizontal plate, while the temperature distribution and concentration of nanoparticle reduce for both flows. On the other hand, the impact of Brownian motion and thermophoresis on the temperature distribution is similar, whereas on the concentration of nanoparticle, the impact is opposite. Further, due to magnetic field, the velocity of fluid increases for Newtonian and non-Newtonian fluids. Larger values of wedge angle parameter lead to enhance the velocity profile and decline the temperature distribution and concentration of nanoparticle. Moreover, temperature difference parameter and dimensionless reaction parameter reduce the concentration of nanoparticle, whereas the profile enhances due to activation energy parameter. Whereas entropy profile is increased due to the greater impact of magnetic field, Reynolds number and Brinkman number, the entropy generation reduces due to Casson parameter. We also observed that the skin friction, Nusselt and Sherwood numbers increase due to higher values of n.

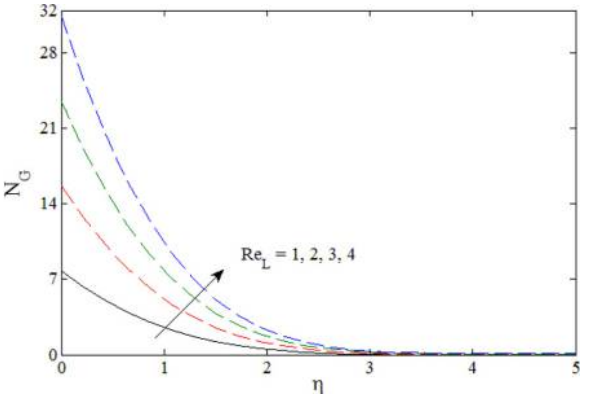

Figure 18.
Entropy generation for different values of Re_L when $\beta = 1, Nt = Nb = 0.1, \gamma = 0.5, M = 0.1, \mathrm{Pr} = Sc = 1, \beta_1 = 3, E = 5, n_1 = 0.5, \delta = 0.5, Br = 1, \zeta = 0.2, \lambda = \Omega = 0.01$

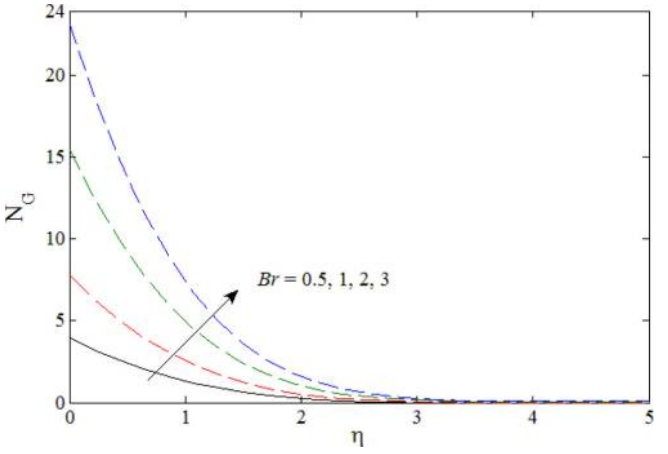

Figure 19.
Entropy generation for different values of Br when $\beta = 1, Nt = Nb = 0.1, \gamma = 0.5, M = 0.1, \mathrm{Pr} = Sc = 1, \beta_1 = 3, E = 5, n_1 = 0.5, \delta = 0.5, \mathrm{Re}_L = 1, \zeta = 0.2, \lambda = \Omega = 0.01$

References

Abolbashari, M.H., Freidoonimehr, N., Nazari, F. and Rashidi, M.M. (2015), "Analytical modeling of entropy generation for casson nano-fluid flow induced by a stretching surface", *Advanced Powder Technology*, Vol. 26 No. 2, pp. 542-552.

Afify, A.A. and Bazid, M.A.A. (2014), "Effects of variable fluid properties on the natural convective boundary layer flow of a nanofluid past a vertical plate: numerical study", *Journal of Computational and Theoretical Nanoscience*, Vol. 11 No. 1, pp. 210-218.

Afify, A.A. and Elgazery, N.S. (2016), "Effect of a chemical reaction on magnetohydrodynamic boundary layer flow of a Maxwell fluid over a stretching sheet with nanoparticles", *Particuology*, Vol. 29, pp. 154-161.

Awad, F.G., Motsa, S. and Khumalo, M. (2014), "Heat and mass transfer in unsteady rotating fluid flow with binary chemical reaction and activation energy", *PLoS ONE*, Vol. 9 No. 9, pp. 1-12.

Bejan, A. (1980), "Second law analysis in heat transfer energy", *Second Law Analysis in Heat Transfer*, Vol. 5 Nos 8/9, pp. 720-732.

Bejan, A. (1996), *Entropy Generation Minimization: The Method of Thermodynamic Optimization of Finite-Size Systems and Finite-Time Processes*, CRC Press.

Bestman, A.R. (1990), "Natural convection boundary layer with suction and mass transfer in a porous medium", *International Journal of Energy Research*, Vol. 14 No. 4, pp. 389-396.

Bhattacharyya, K., Hayat, T. and Alsaedi, A. (2014), "Exact solution for boundary layer flow of casson fluid over a permeable stretching/shrinking sheet", *ZAMM - Journal of Applied Mathematics and Mechanics/Zeitschrift Für Angewandte Mathematik Und Mechanik*, Vol. 94 No. 6, pp. 522-528.

Buongiorno, J. (2006), "Convective transport in nanofluids", *Journal of Heat Transfer*, Vol. 128 No. 3, pp. 240-250.

Cebeci, T. and Bradshaw, P. (1988), *Physical and Computational Aspects of Convective Heat Transfer*, Springer, New York, NY.

Choi, S.U.S. and Eastman, J.A. (1995), "Enhancing thermal conductivity of fluids with nanoparticles", *ASME Fed*, Vol. 231, pp. 99-105.

Durairaj, M., Ramachandran, S. and Rashidi, M.M. (2017), "Heat generating/absorbing and chemically reacting Casson fluid flow over a vertical cone and flat plate saturated with non-darcy porous medium", *International Journal of Numerical Methods for Heat & Fluid Flow*, Vol. 27 No. 1, pp. 156-172.

Freidoonimehr, N., Rashidi, M.M. and Mahmud, S. (2015), "Unsteady MHD free convective flow past a permeable stretching vertical surface in a nano-fluid", *International Journal of Thermal Sciences*, Vol. 87, pp. 136-145.

Galanis, N. and Rashidi, M.M. (2012), "Entropy generation in non-newtonian fluids due to heat and mass transfer in the entrance region of duct", *Heat and Mass Transfer*, Vol. 48 No. 9, pp. 1647-1662.

Hayat, T., Shehzad, S.A., Alsaedi, A. and Alhothuali, M.S. (2012), "Mixed convection stagnation point flow of Casson fluid with convective boundary conditions", *Chinese Physics Letters*, Vol. 29 No. 11, p. 114704

Khan, U., Ahmed, N., Bin-Mohsen, B. and Mohyud-Din, S.T. (2017), "Nonlinear radiation effects on flow of nanofluid over a porous wedge in the presence of magnetic field", *International Journal of Numerical Methods for Heat & Fluid Flow*, Vol. 27 No. 1, pp. 48-63.

Khan, W.A. and Pop, I. (2010), "Boundary-layer flow of a nanofluid past a stretching sheet", *International Journal of Heat and Mass Transfer*, Vol. 53 Nos 11/12, pp. 2477-2483.

Liu, Z., Liu, Y., Chang, Y., Seyf, H.R., Henry, A., Mattheyses, A.L., Yehl, K., Zhang, Y., Huang, Z. and Salaita, K. (2016), "Nanoscale optomechanical actuators for controlling mechanotransduction in living cells", *Nature Methods*, Vol. 13 No. 2, pp. 143-146.

McDonald, D.A. (1974), *Blood Flows in Arteries*, 2nd ed., Chapter 2, Arnold, London.

Mahmud, S. and Fraser, R.A. (2004), "Magnetohydrodynamic free convection and entropy generation in a square porous cavity", *International Journal of Heat and Mass Transfer*, Vol. 47 Nos 14/16, pp. 3245-3256.

Maleque, K.A. (2013), "Effects of binary chemical reaction and activation energy on MHD boundary layer heat and mass transfer flow with viscous dissipation and heat generation/absorption", *ISRN Thermodyn*, Vol. 2013, pp. 1-7.

Malik, M.Y., Salahuddin, T., Hussain, A. and Bilal, S. (2015), "MHD flow of tangent hyperbolic fluid over a stretching cylinder: using Keller box method", *Journal of Magnetism and Magnetic Materials*, Vol. 395, pp. 271-276.

Mousavi, S.M.R. and Abbasbandy, S. (2011), "Analysis of forced convection in a circular tube filled with a darcy-brinkman-forchheimer porous medium using spectral homotopy analysis method", *Journal of Fluids Engineering*, Vol. 133 No. 10, pp. 101207-101209.

Mousavi, S.M.R. and Yaghoobi, H. (2014), "Effect of non-linear drag term on viscous dissipation in a fluid saturated porous medium channel with various boundary conditions at walls", *Arabian Journal for Science and Engineering*, Vol. 39 No. 2, pp. 1231-1240.

Mousavi, S.M.R., Seyf, H.R. and Abbasbandy, S. (2013), "Heat transfer through a porous saturated channel with permeable walls using two-equation energy model", *Journal of Porous Media*, Vol. 16 No. 3, pp. 241-254.

Mousavi, S.M.R., Abbasbandy, S. and Alsulami, H.H. (2014), "Analytical flow study of a conducting maxwell fluid through a porous saturated channel at various wall boundary conditions", *European Physical Journal - Plus*, Vol. 129, pp. 1-10.

Mousavi, S.M.R., Mao, Y. and Zhang, Y. (2014), "Evaluation of copper, aluminum, and nickel interatomic potentials on predicting the elastic properties", *API Journals Applied Physics*, Vol. 119 No. 24, pp. 244304.

Mustafa, M., Hayat, T., Pop, I. and Hendi, A.A. (2012), "Stagnation-point flow and heat transfer of a casson fluid towards a stretching sheet", *Z. Naturforsch*, Vol. 67, pp. 70-76.

Mutlag, A.A., Uddin, M.J., Hamad, M.A.A. and Ismail, A.I. (2013), "Heat transfer analysis for falkner-skan boundary layer flow past a stationary wedge with slips boundary conditions considering temperature-dependent thermal conductivity", *Sains Malaysia*, Vol. 42, pp. 855-862.

Nield, D.A. and Kuznetsov, A.V. (2009), "The cheng-minkowycz problem for natural convective boundary-layer flow in a porous medium saturated by a nanofluid", *International Journal of Heat and Mass Transfer*, Vol. 52 Nos 25/26, pp. 5792-5795.

Nield, D.A. and Kuznetsov, A.V. (2010), "Natural convective boundary-layer flow of a nanofluid past a vertical plate", *International Journal of Thermal Sciences*, Vol. 49, pp. 243-247.

Qing, J., Bhatti, M.M., Abbas, M.A., Rashidi, M.M. and Ali, M.E.S. (2016), "Entropy generation on MHD Casson nanofluid flow over a porous stretching/shrinking surface", *Entropy*, Vol. 18 No. 4, p. 123.

Rashidi, M.M., Kavyani, N. and Abelman, S. (2014), "Investigation of entropy generation in MHD and slip flow over a rotating porous disk with variable properties", *International Journal of Heat and Mass Transfer*, Vol. 70, pp. 892-917.

Seyf, H.R. and Mousavi, S.M.R. (2011), "An analytical study for fluid flow in porous media imbedded inside a channel with moving or stationary walls subjected to injection/suction", *Journal of Fluids Engineering*, Vol. 133 No. 9, doi: 091203-091203-9.

Shateyi, S., Motsa, S.S. and Makukula, Z. (2015), "On spectral relaxation method for entropy generation on a MHD flow and heat transfer of a maxwell fluid", *Journal of Aplied Fluid Mechanics*, Vol. 8, pp. 21-31.

Shaw, S., Gorla, R.S.R., Murthy, P.V.S.N. and Ng, C.O. (2009), "Pulsatile casson fluid flow through a stenosed bifurcated artery", *International Journal of Fluid Mechanics Research*, Vol. 36 No. 1, pp. 43-63.

Shehzad, S.A., Hayat, T., Qasim, M. and Asghar, S. (2013), "Effects of mass transfer on MHD flow of casson fluid with chemical reaction and suction", *Brazilian Journal of Chemical Engineering*, Vol. 30 No. 1, pp. 187-195.

Shirazpour, A., Mousavi, S.M.R. and Seyf, H.R. (2011), "HPM solution of momentum equation for darcy-brinkman model in a parallel plates channel subjected to Lorentz force", *International Conference on Fluid Mechanics, Heat Transfer and Thermodynamics*, Vol. 5, pp. 258-262.

White, F.M., (1991), *Viscous Fluid Flow*, 2nd ed., McGraw-Hill, New York, NY.

Yacob, N.A., Ishak, A. and Pop, I. (2011), "Falkner-skan problem for a static or moving wedge in nanofluids", *International Journal of Thermal Sciences*, Vol. 50 No. 2, pp. 133-139.

Yih, K.A. (1998), "Uniform suction/blowing effect on forced convection about a wedge: uniform heat flux", *Acta Mechanica*, Vol. 128 Nos 3/4, pp. 173-181.

Zaib, A., Bhattacharyya, K., Uddin, M.S. and Shafie, S. (2016), "Dual solutions of non-Newtonian Casson fluid flow and heat transfer over an exponentially permeable shrinking sheet with viscous dissipation", *Modeling and Simulation in Engineering*, Vol. 2016, pp. 1-8.

Corresponding author
Aurang Zaib can be contacted at: zaib20042002@yahoo.com